Phase plane approach to cooperative rhythms in neuron motifs with delayed inhibitory synapses

2010 EPL 92 68007

(http://iopscience.iop.org/0295-5075/92/6/68007)

A Letters Journal Exploring the Frontiers of Physics

December 2010

EPL, **92** (2010) 68007
doi: 10.1209/0295-5075/92/68007

www.epljournal.org

Phase plane approach to cooperative rhythms in neuron motifs with delayed inhibitory synapses

I. Franović and V. Miljković[(a)]

Faculty of Physics, University of Belgrade - P.O. Box 368, 11001 Belgrade, Serbia

received 29 June 2010; accepted in final form 8 December 2010
published online 24 January 2011

PACS 87.18.Sn – Neural networks and synaptic communication
PACS 05.45.Xt – Synchronization; coupled oscillators
PACS 87.19.ll – Models of single neurons and networks

Abstract – The phenomenon of burst synchronization is analyzed in binary and ternary motifs consisting of Rulkov map neurons coupled via delayed inhibitory synapses. We determine the particular roles and the interplay between the intrinsic neuron and synaptic parameters, as well as the network topology. The developed method, resting on exactly obtaining the curves that guide the neuron orbits in the phase plane, enabled us to identify the motif-specific mechanisms of how the synchronized rhythms emerge, even in the presence of strong delay. It is explained why the location of the parameter space domain optimal for burst synchronization gets shifted with different motif architectures. Further, it is suggested how for each motif a distinct cooperative rhythm may be singled out, that is absent on any of the other considered motifs.

Introduction. – The recent research has provided compelling evidence that the structure of complex networks rests on repetition of elementary building blocks, network motifs [1], whose connectivity patterns are significantly over-represented when compared to a randomized network configuration with the same nodal degree distribution. Moreover, in neural networks [2,3], such small circuits seem to act in an independent manner [4], as implied by the generally stronger intra- than inter-motif synaptic weights. Due to findings in several brain areas [5,6] and in CPGs [7], the setup attracting considerable interest has been the one where the participant neurons are endogenous bursters. They engage in coordinated activity, that may be studied embracing the concept of chaotic phase synchronization [8]. One of its manifestations is burst synchronization [9–11], which involves matching between the respective times of onset and termination of bursts.

The establishing of synchronous rhythms is guided by the synergetic action of the intrinsic and synaptic parameters, as well as the network topology [10,12]. In that respect, it is plausible to consider the reciprocal inhibition, widespread in the common motifs, and to include the possibility of transmission delays, whose range may cover both the cases of activity in local networks, exhibiting no or small delay, and the simplification of cooperative activity between the more distributed brain regions (larger delay), like in the cortico-thalamo-cortical loop [13]. Given the present body of work on the effects of inhibitory synapses and the transmission delay in synchronization phenomena [12,14,15], our study focuses on two points. First, it concerns the exact roles and the interplay between the intrinsic and the synaptic parameters, *e.g.* the basic relationship between the transmission delay and the synaptic weight, and second, the possibility of anticipating the domains of parameter space where different types of coordinated activity are most likely to occur.

Though phenomenological, the Rulkov map neuron model [16,17], accompanied with the sufficiently detailed model of the delayed chemical synapse, provides an appropriate setting to explore the first point. To do so, we develop the phase plane approach [18], that essentially presents the analysis of geometrical implications derived from the theory of coupled systems with singular perturbation [19]. It consists in monitoring the switching dynamics between the noninteracting and the various interacting maps, making advances in understanding of the mechanisms by which the synchronization regimes are shaped. Further, the variation of the quantity H, introduced to characterize the degree of burst synchronization, provides an indication on how the parameters should be adjusted to achieve better neuron coordination.

[(a)] E-mail: vladimir.miljkovic@ff.bg.ac.rs

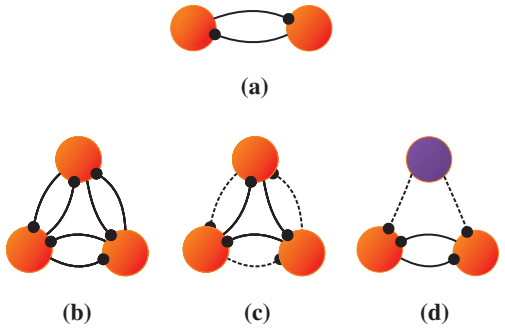

Fig. 1: (Colour on-line) Schematic representation of the considered motifs, with circles denoting the neurons, and dots standing for the synapses. (a) Binary and (b) ternary inhibitory motifs with symmetrical couplings, each assigned the weight g_c. (c) Asymmetrical inhibitory motif, where the connections in clockwise (solid lines) and counterclockwise (dashed lines) assume weights g_{c1} and g_{c2}, respectively. (d) Ternary motif with the pacemaker, displayed in blue (dark grey), and the driven neurons, presented by red (light grey). Mutual couplings between the driven neurons (solid lines) take the weights g_c, whereas the couplings from the pacemaker (dashed lines) attain g_{cp}.

Finally, we are interested in assessing the ways in which changing network topology affects the formation of novel cooperative rhythms. To this end, four network configurations are considered, corresponding to the most common binary and ternary inhibitory motifs [2,4], with the details presented in fig. 1.

Model. – The dynamics of the coupled neuron i follows a two-dimensional map

$$\begin{aligned} x_{i,n+1} &= \frac{\alpha}{1+x_{i,n}^2} + y_{i,n} \\ &\quad - \sum_{j\in nn} g_{c,ij}(x_{i,n}-\nu)\,\frac{1}{1+\exp(-k(x_{j,n-\tau}-\theta))}, \\ y_{i,n+1} &= y_{i,n} - \mu(x_{i,n}-\sigma), \end{aligned} \tag{1}$$

where the summation over the presynaptic neurons j is motif dependent, and n denotes the iteration step. Without the interaction term, eq. (1) reduces to chaotic Rulkov map that, with the appropriate choice of parameters, yields square-wave bursts. Setting $\mu = 0.001$, the neuron state is defined by the fast variable $x_{i,n}$ and the slow variable $y_{i,n}$, the former of which embodies the membrane potential, and the action of the latter is reminiscent of that of the gating variables. A brief reminder on the ensuing analysis for the isolated neuron, treating $y_{i,n}$ as a control parameter γ within the fast subsystem, is presented in fig. 2, and for a comprehensive review one may consult [11,17]. Here we briefly note that the phase point motion is guided by the fast nullclines, merged in an S-curve, and the curves of minimal and maximal map iterates, Ξ_{min} and Ξ_{max}, providing the burst envelopes. In effect, bursting dynamics relies on the existence of the bistability region in the fast subsystem that arises if

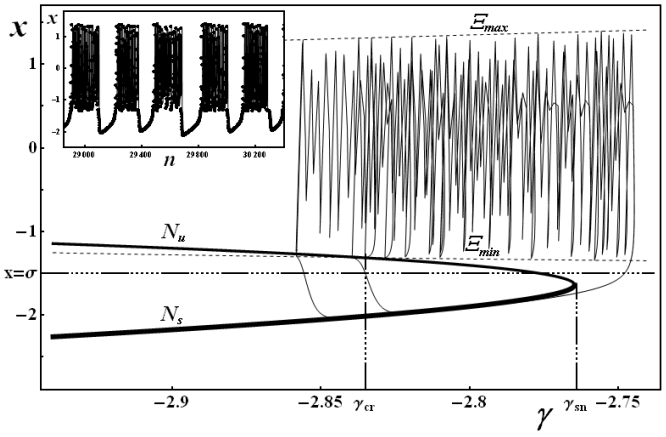

Fig. 2: Blowup of the bistability region of the fast subsystem. Bursting is enabled if the slow variable nullcline $x_n = \sigma$ intersects the branch of unstable fixed points N_u. γ increases (decreases) whenever the phase point lies below (above) the slow nullcline. Phase point climbing along the stable branch N_s coincides with the interburst intervals, whereas the bursts are delimited by the points of the saddle-node bifurcation $\gamma = \gamma_{sn}$ and the external crisis $\gamma = \gamma_{cr}$. The irregularity of the series comes from the termination delay beyond γ_{cr}. The inset displays a typical bursting sequence of the isolated neuron obtained for $\alpha = 4.15$ and $\sigma = -0.9$.

$\alpha > 4$. One may also use α to control the irregularity of bursts: the closer α gets to 4, the less chaotic the bursting series becomes. With a single exception, throughout the paper we select $\alpha = 4.15$, the value providing a reasonable balance between the bursts' duration and the stochasticity due to their termination delay. Unless specifically stated, the external dc bias current σ, affecting the length of the neuron's duty cycle, is assumed homogeneous within a motif ($\sigma = -0.9$).

Moving onto the interaction term, the reversal potential [5] $\nu = -1.8$ is set so as to give the synapses the inhibitory character, whereas the synaptic weights $g_{c,ij}$ depend on the particular circuit configuration. The time lag τ, equal over the synapses, is reflected by the delayed arrival of the presynaptic potential influencing the gate opening. Within the sigmoid, for the activation threshold is chosen $\theta = -1.4$, a value easily reached by the bursting neuron. The sharpness of the synaptic response is determined by the gain parameter k [9,14,20]. The $k \gg 1$ case yields the fast threshold modulation model [21], approximating well the action of the majority of chemical synapses in the brain [18,22], while for $k \sim 1$ one obtains the graded synaptic transmission model [23], appropriate to the description of the CPGs. Hereafter, we keep $k = 25$ fixed, since the dynamics of a system with higher k is more amenable to the type of analysis to follow.

Along the phase plane approach in terms of tracing the motion of the phase point, in the following we introduce the quantity appropriate to characterize how the level of burst synchronization depends on the neuron and synaptic parameters. To this end, it is convenient to transform

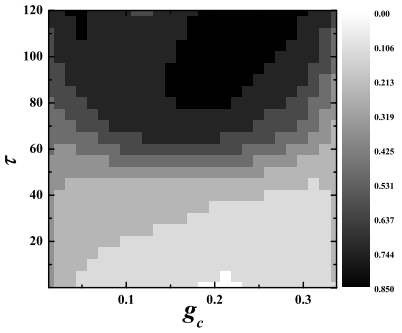

Fig. 3: Quantity H for the binary motif in the (g_c, τ)-plane, with the higher values reflected by the darker shading. Though larger delays generally favor burst synchronization, only the interplay with g_c ensures the existence of the DMS (black region), where the two neurons are typically synchronized in phase.

the time series of the interacting neurons' membrane potentials into symbolic sequences $\{S_{i,n}\}$. We apply a conversion rule T that ascribes $S_{i,n} = 1$ if the neuron is bursting, and -1 otherwise:

$$S_{i,n} = T(x_{i,n}) = \begin{cases} 1, & x_{i,n} \text{ in the bursting range;} \\ -1, & x_{i,n} \text{ in the silence range.} \end{cases} \tag{2}$$

It turns out that a useful rule of thumb to determine when a burst is triggered or terminated is to identify the moments when $x_{i,n}$ crosses θ from below and from above, respectively. Next, as a measure of burst synchronization between the two neurons i and j, we define the quantity

$$H_{ij} = \frac{1}{N_{max}} \left\langle \sum_{n=1}^{N_{max}} \delta(S_{i,n}, S_{j,n}) \right\rangle, \tag{3}$$

where δ represents the Kronecker symbol, and $N_{max} = 50000$ steps is the length of the observed time series. The angled brackets in eq. (3) refer to averaging over 100 trials with different initial conditions. H (the indices are dropped for simplicity) can be understood as a trial-averaged fraction of time in which the symbolic sequences of the two neurons overlap. This means $H \in [0, 1]$ holds, whereby the larger values correspond to higher burst synchronization. We note that the value $H = 1$ would not imply that the exact synchronization has been reached, but the values less than 1 are sufficient to rule it out.

Binary motif. – The form of interaction considered here allows the curve of fixed points to maintain the S-shape and the stability features, with the map itself shifted rightward and upward in the phase plane. Hence the establishing of cooperative bursting rhythms can be explained by observing the motion of the neurons' phase points, whose dynamics consists of switches between the isolated and the motif-specific coupled (interacting) maps.

Without the delay, the neuron activity is prevailingly coordinated in the regime of anti-phase synchronization, which improves if the difference between the durations of

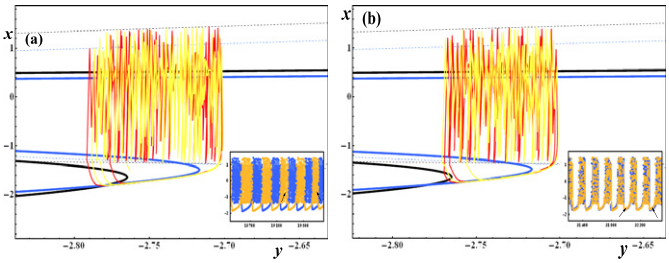

Fig. 4: (Colour on-line) Phase plane analysis for the inhibitory couple in case $g_c = 0.2$. The non-interacting and the interacting S-curves, with the corresponding envelopes, are presented by black and blue (dark grey) solid and dashed lines, respectively. The main frames show the neuron waveforms in yellow (lightest grey) and red (grey). (a) When τ is small, typically there is anti-phase synchronization, illustrated by the inset sequence for $\tau = 10$, with the neurons coded in blue (dark grey) and orange (light grey). The section between the arrows is extracted to the main frame. (b) The increase of τ promotes in-phase synchronization. The data obtained for $\tau = 90$ are displayed in the same way as in (a).

the burst and the interburst intervals becomes smaller, depending on synaptic weights. In the approximately ideal case when this difference is the smallest ($0.19 \lesssim g_c \lesssim 0.23$, cf. the bottom white region in fig. 3), the anti-phase synchronization follows the lock-and-release mechanism [10,22], so that the given neuron, say neuron 2, becomes active as soon as 1 terminates its burst ($x_1 < \theta$), releasing 2 from inhibition. Translated into the phase plane, this means that the neuron bursts according to the isolated map, and that it spends the interburst interval on the stable branch of the coupled map, leaving it in the vicinity of the saddle-node, see fig. 4(a). For higher g_c, there is imperfect anti-phase synchronization, where the neuron begins to burst by the escape mechanism [22], moving beyond the saddle-node of the coupled map before the other neuron ceases to burst.

Introducing the synaptic delay, such a regime is maintained in a broader g_c interval, whereby the escape mechanism gets "regularized", in a sense that the beginning of one neuron's burst prompts the other neuron's burst to terminate with the τ steps delay. Compared to the action of the instantaneous synapses, the bursts' length changes negligibly, but the delay influence manifests in a way that a part of the burst, 2τ steps long, takes place on the coupled map, cf. fig. 5(a). Increasing τ, this picture is preserved till the values given by the curve $\tau_{SH}(g_c)$ (see fig. 5(b)), when the section of the burst on the coupled map reaches its external crisis. Then the two scenarios may arise: either the phase point drops below the external crisis or the burst continues, so that the phase point moves from the chaotic attractor of the coupled map onto the one of the isolated map, exhibiting a heteroclinic trajectory near the saddle fixed point of the isolated map. Due to the first scenario, for $\tau > \tau_{SH}(g_c)$, in the time series one observes the occurrence of short, phase-synchronized bursts approximately

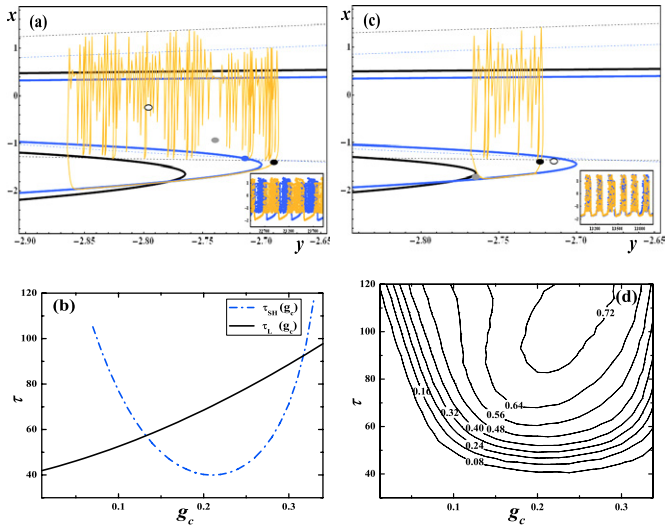

Fig. 5: (Colour on-line) (a) Typical waveform of a long burst, obtained for $g_c = 0.2$ and $\tau = 65$, is embedded in the phase plane, with the ensuing time sequence shown in the inset. When the neuron begins the burst (black bullet), the other neuron, still bursting, is in site of the empty bullet, but its phase point is "seen" with a τ step delay (grey bullet). The blue (dark grey) bullet on the coupled map presents its external crisis. (b) The $\tau_{SH}(g_c)$ curve (dash-dotted line) marks the approximate lower boundary for the occurrence of short bursts, whereas above $\tau_L(g_c)$ (solid line) the number of long bursts diminishes. (c) A display of a typical short burst, extracted from the same series as the long burst, using the form of presentation adopted from (a). (d) Contours show constant fraction of short bursts within the time series, plotted in the (g_c, τ) parameter plane. The contours were obtained averaging over 200 independent runs.

τ steps long, which follow the "release" mechanism [22] of bursting, so dubbed as the neuron jumps off the coupled map at the moment it "sees" the other neuron falling below θ (fig. 5(c)). Along the short bursts, the time series still contain the sequences of long bursts as remnants of the regime of anti-phase synchronization. The burst length fluctuations reduce considerably when the delay reaches $\tau_L(g_c)$ (see fig. 5(b)), since the sequential occurrence of long bursts becomes less likely. This curve is determined so as to characterize the turning point when the parts of burst on the isolated and the coupled map are equal to 2τ steps each, which makes the last sustainable waveform of long bursts for the given g_c. In reference to fig. 3, the area $\tau_{SH}(g_c) < \tau < \tau_L(g_c)$ coincides with the moderate values of H, whereas the curve $\tau_L(g_c)$ roughly presents the lower edge of the domain of maximal synchronization (DMS), where the neurons are typically synchronized in phase. Within the DMS, the long bursts do not completely disappear. However, the increase of τ causes the fraction of short bursts within the series to grow (see fig. 5(d)) on account of the long ones, becoming the largest in the region almost overlapping with the DMS. Nonetheless, moving toward the inner area of the latter, for rising τ it is seen that the onset of short bursts, except by

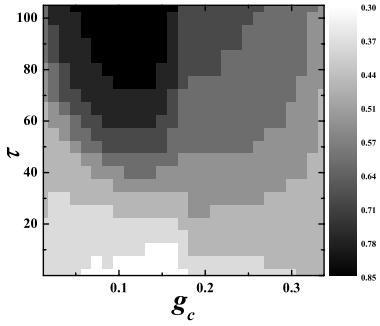

Fig. 6: For the symmetrical ternary motif, the variation of H for an arbitrary pair of neurons is considered.

the release mechanism, increasingly occurs by the escape mechanism, as shown in fig. 4(b).

Ternary motifs. – Applying the introduced methods, we analyze the mutual synchronization on the ternary motifs, allowing the possibilities of weight heterogeneity and different connection topologies. First we discuss the extension of the binary to the symmetrical ternary motif, where it is sufficient to observe the variation of H in the (g_c, τ)-plane for an arbitrary pair of neurons (fig. 6). The DMS here is distinguished from the one in fig. 3 insofar as it is centered around smaller weights, $g_c \approx 0.1$, and, notably, signifies the area where all three neurons become synchronized in phase. In the phase plane, such a regime is guided by the action of three maps, that correspond to the isolated neuron, onefold and the twofold inhibited neuron. In an ideal case, the three neurons should burst by the isolated map, and the interburst intervals would coincide with the motion along the stable branch of the twofold interacting $(2g_c)$ map. Performing the kind of analysis presented in fig. 5(b), one can demonstrate a change in shape and slope of the relevant curves, which accounts for the shift in location and the different inclination of the DMS in case of the ternary as opposed to the binary motif.

Now let us consider the motif with rotationally invariant asymmetrical synapses, assigning the weights in clockwise direction g_{c1}, and those in counterclockwise direction g_{c2}. Based on this setup, one should anticipate the appearance of rotating waves [24], here observed as a winnerless rhythm with alternation of the bursting neuron (fig. 7(a)), also known as the $\frac{2\pi}{3}$ resonance [10]. To achieve such a rhythm, one is required to change the intrinsic parameters α and σ, so as to reduce the burst irregularity, *e.g.* by decreasing α to 4.05, and the neuron duty cycle, *e.g.* by choosing $\sigma = -1.2$. Insofar as the synaptic parameters are concerned, to maintain the waves, there should be no or very small delay, say $\tau = 10$. For each selection of (g_{c1}, g_{c2}) the waves can propagate in either of the directions, this being influenced by the initial conditions of the motif. Nonetheless, one finds the areas where such influence is manifested less, so that the rotation in the direction of the weaker (RWS) or stronger synapses (RSS) is preferred, cf. fig. 7(b), whereas in most of the parameter plane

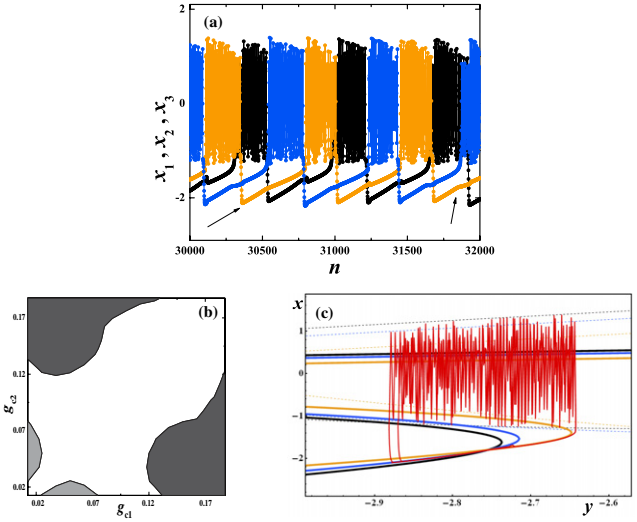

Fig. 7: (Colour on-line) Anti-phase synchronization on the asymmetrical motif is achieved for $\alpha = 4.05$. (a) The respective neuron time series are presented by black, blue (dark grey) and orange (light grey). The data are obtained for $g_{c1} = 0.1$, $g_{c2} = 0.3$ and $\tau = 10$. (b) For $\tau = 10$, in the (g_{c1}, g_{c2}) parameter plane are displayed the areas with the prevailing RWS (light grey) or RSS (dark grey) direction of waves, whereas the largest domain, shown white, coincides with the case where both directions occur with similar probabilities. (c) The neuron's sequence, marked by the arrows in (a), is embedded in the phase plane. The non-interacting map and the two interacting maps corresponding to g_{c1} and g_{c2} are presented by black, blue (dark grey) and orange (light grey) lines, respectively.

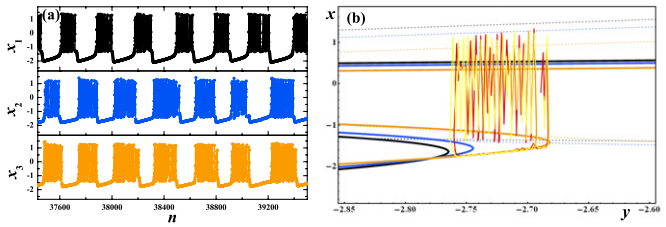

Fig. 8: (Colour on-line) Burst synchronization between the driven neurons under the influence of the pacemaker. (a) The pacemaker series, shown black, lies in anti-phase with the sequences of the driven neurons, displayed by blue (dark grey) and orange (light grey). The data are obtained for $g_c = 0.1$, $g_{cp} = 0.3$ and $\tau = 10$, with the stimulus on pacemaker $\sigma_p = -0.9$, and on the driven neurons $\sigma = -1.2$. (b) The superimposed sequences correspond to the driven neurons, whereas the non-interacting map and the two interacting maps, g_c and g_{cp}, are presented by black, blue (dark grey) and orange (light grey) lines, respectively.

the rotation direction is strongly sensitive to the initial conditions. The actual shape of these domains changes with τ, as the prevailingly unidirectional areas get smaller, giving way to the bidirectional area in between. It can also be demonstrated that for the RWS (RSS), considering different initial conditions, the average burst duration, determined by the coupling strengths, is shorter (larger) than the one for the isolated neuron [25], while in the rest of the parameter plane this average is approximately equal to the length obtained for the autonomous bursts. In case when the stronger inhibited neuron fires next (RSS direction), the phase plane (fig. 7(c)) shows a curious interplay between the isolated map and the g_{c1} and g_{c2} coupled maps. In effect, the bursting period is split into three approximately equal parts, whereby the burst, following the isolated map, comprises only a third of the period. The interburst interval coincides with the motion of the phase point along the stable branches of the two interacting maps, first subjected to the weaker of the synapses, and then the stronger one.

The final circuit we consider consists of three neurons, two of which are symmetrically coupled, receiving the common inhibition from the third neuron, the pacemaker. This configuration has been identified among the most frequently represented motifs [4,26], and is here dubbed in reference to the study of CPGs [12,27]. Given the connection topology, it comes natural to assume the stimulus heterogeneity, whereby the reason for selecting the duty cycle of the pacemaker longer than the driven neurons ($\sigma_p > \sigma$) will become clear below. Compared to the binary motif, there is a qualitatively new occurrence of burst synchronization between the driven neurons at small τ, that arises under the action of the pacemaker. In this regime, the pacemaker lies in anti-phase with the driven neurons (fig. 8(a)), implying the importance of the relative positions of the g_c and g_{cp} interacting maps in the phase plane (fig. 8(b)). On the other hand, distinguishing from the symmetrical three-node motif, burst synchronization of the driven neurons is not contributed by the joint inhibition, that is the $g_c + g_{cp}$ map. Herein, silence of the driven neurons coincides with the climbing of the phase point along the stable branch of the g_{cp} map, whereas bursting takes place between the envelopes defined by the g_c map. This gives an insight into how g_{cp} and g_c should be adjusted: $g_{cp} > g_c$ is necessary to hold, so that the motion along the stable branch of the g_{cp} map covers the entire bursting interval of the pacemaker.

In light of the previous motif configurations, to consider the effects on dynamics mediated by the stronger delay, we examine the variation of the quantity H for the driven neurons in the (g_c, τ)-plane, keeping g_{cp} fixed (see fig. 9(a)). One observes a non-trivial effect of the time delay: there is an area of high burst synchronization for $\tau > 60$, even in case $g_{cp} < g_c$. We further confirmed this by determining H in the (g_c, g_{cp})-plane for the two selected delay values, $\tau = 10$ (fig. 9(b)) and $\tau = 90$ (fig. 9(c)). As opposed to the former, in the latter case the area of high synchronization makes an incursion beyond the identity line, partly due to the burst duration of the driven neurons being controlled by τ. Then the time series assumes very specific form (see fig. 9(d)), that involves repetitive cycles where, during the two bursts of the pacemaker, the driven neurons burst three times. In an ideal case, the middle burst of the driven neurons fits in the interburst interval of

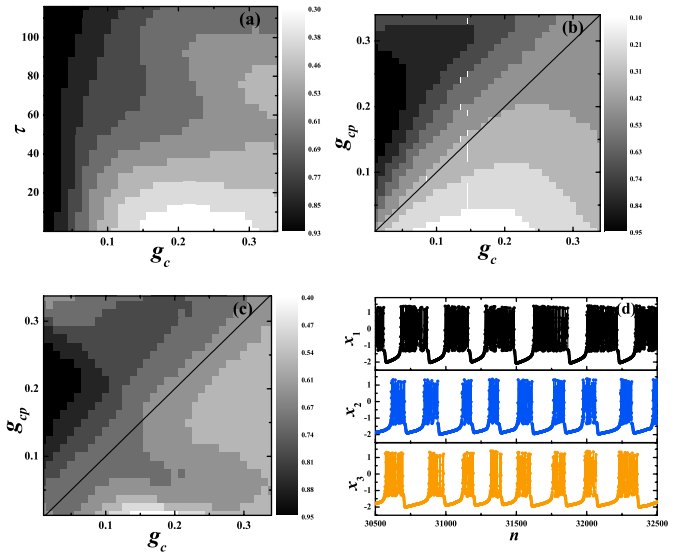

Fig. 9: (Colour on-line) Extensive exploration of burst synchronization for the motif with pacemaker. (a) H-dependence for the driven neurons in the (g_c, τ)-plane with g_{cp} fixed at 0.15. The stimulus to pacemaker $\sigma_p = -0.9$ is stronger than the one on the driven neurons ($\sigma = -1.2$). (b) For $\tau = 10$ the driven neurons are synchronized in phase only for $g_{cp} > g_c$. (c) For $\tau = 90$ burst synchronization between the driven neurons is also possible if $g_{cp} < g_c$. (d) From top to bottom are displayed the respective waveforms of the pacemaker and the driven neurons, obtained for $\tau = 90$ and $(g_c, g_{cp}) = (0.14, 0.08)$.

the pacemaker, which requires $\sigma_p > \sigma$ be fulfilled. Since the phase plane dynamics becomes more involved, it suffices to say that in contrast to the previous cases, synchronization in phase between the bursts takes place on the coupled map, specifically the one for g_{cp}.

Summary. – What we presented so far implies that the phase plane analysis may serve as a shortcut in understanding the relation between the modulated dynamics on a single neuron level and the activity of the coupled system. This is upheld for any of the considered motifs, but it is easiest to summarize in case of the binary one, where the bursting series of a neuron reduces to a virtual two-state dynamics, such that the occurrence and the increasing number of short bursts give rise to H, the quantity introduced to characterize the degree of burst synchronization. In case when the asymmetry of synaptic weights and/or stimuli is involved, the phase plane approach enabled us to explain how the change of parameters influences the coexistence and the succession between the different regimes of coordinated neuron activity. On the point of topology, it stands out that along with the rhythms shared between the motifs, one also finds a unique rhythm, specific for each motif configuration. Whether an analogy to this can be extended if the conductance-based neuron models are implemented remains to be seen, but so far it is known that the winnerless rhythm in the asymmetrical motif [10] and burst synchronization between the driven neurons in the pacemaker motif [12] exist under conditions similar to ours when coupling the Hodgkin-Huxley neurons. Thinking ahead, the research presented may open the way toward identifying the functional motifs and analyzing their interactions in larger networks.

* * *

This research was performed as part of the work within project No. 141020, funded by the Serbian Ministry of Science and Technological Development.

REFERENCES

[1] Milo R. *et al.*, *Science*, **298** (2002) 824; Alon U., *Nature*, **8** (2007) 450.
[2] Sporns O. and Kotter R., *PLoS Biol.*, **2** (2004) e369.
[3] Song S. *et al.*, *PLoS Biol.*, **3** (2005) e68.
[4] Li C., *Phys. Rev. E*, **78** (2008) 037101.
[5] Ibarz B., Cao H. and Sanjuán M. A. F., *Phys. Rev. E*, **77** (2008) 051918.
[6] Ivanchenko M. V. *et al.*, *Phys. Rev. Lett.*, **93** (2004) 134101.
[7] Elson R. C. *et al.*, *Phys. Rev. Lett.*, **81** (1998) 25; Elson R. C. *et al.*, *J. Neurophysiol.*, **88** (2002) 1166.
[8] Schimansky-Geier L., Anishchenko V. S. and Neiman A., in *Neuro-informatics and Neural Modelling*, edited by Moss F. and Gielen S. (Elsevier, Amsterdam) 2001.
[9] Belykh I., de Lange E. and Hasler M., *Phys. Rev. Lett.*, **94** (2005) 188101.
[10] Shilnikov A., Gordon R. and Belykh I., *Chaos*, **18** (2008) 037120.
[11] Franović I. and Miljković V., *Eur. Phys. J. B*, **76** (2010) 613.
[12] Belykh I. and Shilnikov A., *Phys. Rev. Lett.*, **101** (2008) 078102.
[13] Vicente R. *et al.*, *Proc. Natl. Acad. Sci. U.S.A.*, **105** (2008) 17157; Jones E., *Philos. Trans. R. Soc. B*, **357** (2002) 1659.
[14] Burić N., Todorović K. and Vasović N., *Phys. Rev. E*, **78** (2008) 036211.
[15] Wang Q. *et al.*, *EPL*, **83** (2008) 50008; Rossoni E. *et al.*, *Phys. Rev. E*, **71** (2005) 061904.
[16] Rulkov N. F., *Phys. Rev. Lett.*, **86** (2001) 183.
[17] de Vries G., *Phys. Rev. E*, **64** (2001) 051914.
[18] Arbib M. A. (Editor), *Handbook of Brain Theory and Neural Networks* (MIT Press, Cambridge) 2003.
[19] Terman D. *et al.*, *Physica D*, **237** (2008) 324.
[20] Rowat P. F. and Selverston A. I., *J. Comput. Neurosci.*, **4** (1997) 103.
[21] Somers D. and Koppel N., *Biol. Cybernet.*, **68** (1993) 393.
[22] Koppel N. and Ermentrout G. B., in *Handbook of Dynamical Systems*, edited by Fiedler B. (Elsevier, Amsterdam) 2002.
[23] Varona P. *et al.*, *Neural Netw.*, **14** (2001) 865.
[24] Stewart I., Golubitsky M. and Pivato M., *SIAM J. Appl. Dyn. Syst.*, **2** (2003) 609.
[25] Ivanchenko M. V. *et al.*, *J. Theor. Biol.*, **253** (2008) 452.
[26] Reigl M., Alon U. and Chklovskii D. B., *BMC Biol.*, **2** (2004) 25.
[27] Mouser C., Nadim F. and Bose A., *J. Math. Biol.*, **57** (2008) 161.